

Novel Nanostructured Zn-substituted Monetite Based Biomaterial for Bone Regeneration

Sussette Padilla^{1*}, Arcadio García de Castro¹, Ana Garzón-Gutiérrez¹, Lorena Benito², Silvia Enciso³, María Canillas⁴ and Raúl G Carrodeguas¹

¹AzureBio SL, Tres Cantos, Madrid, Spain

²Departamento de Cirugía, Facultad de Medicina, Universidad de Salamanca, Salamanca, España

³Centro de Cirugía de Mínima Invasión Jesús Usón, Cáceres, Spain

⁴Instituto de Cerámica y Vidrio - CSIC, Cantoblanco, Madrid, Spain

Abstract

A bone regeneration biomaterial must be biocompatible, osteoconductive and osteoinductive, and be gradually replaced by newly formed bone in the shorter time possible. Nanostructured materials, emulating bone composition and morphology, have shown great potential in bone repair because of their higher reactivity, faster reabsorption and improved biological behavior over microstructured materials.

This work was aimed at developing a new biomaterial that meets the requirements for effective bone regeneration. Combination of components with different solubility such as monetite, hydroxyapatite, amorphous calcium phosphate and silica gel, provided with the means to modulate the rate of material resorption of this novel biomaterial were Zn was found to be present as a partial substitution of Ca in the monetite lattice. The biomaterial was obtained by a hydraulic cementing reaction and was characterized by XRD, FTIR, NMR, chemical analysis, N₂ adsorption porosimetry, Hg porosimetry, picnometry, SEM, TEM and evaluated *in vitro* and *in vivo*.

Granular biomaterial showed a nanometric structure with a very high specific surface area (≈ 80 m²/g), high surface roughness and high intragranular porosity (50%) ranging from macro to nanopores. All of these are key features for a bone regeneration material. Solubility studies demonstrate the different solubility of its components and the release of Ca, P, Si and Zn. *In vivo* evaluation showed the effectiveness of the material to regenerate and to maintain 89 \pm 9% of the volume of a critical size bone defect in sheep at 16 weeks. Residual biomaterial was found to occupy 10 \pm 5% of the defect while newly formed trabeculae occupied 35 \pm 6% of the space. The newly formed bone showed abundant vascularization and osteogenic activity. Biomaterial was estimated to have resorbed by 85 \pm 7% with a reduction of 67 \pm 8% in area and clear signs of cell-mediated resorption.

Keywords: Monetite; Hydroxyapatite; Silica; Zinc; Amorphous calcium phosphate; Nanometric; Nanostructured; Solubility; Resorption; Bone regeneration

Introduction

Bone tissue is under continuous turn-over involving resorption of bone by osteoclasts and formation of new bone by osteoblast. This bone remodeling process provides the means for self-regeneration after injury and for the continuous adaptation of bone mass and its architecture to the prevailing mechanical load [1]. However, this regenerative capacity is limited to small defects, with larger defects often requiring surgical intervention involving bone grafts. Common bone grafts include bone autografts obtained from the same patient (autologous bone), allografts, originating from a different individual, animal derived xenografts and synthetic bone graft substitutes. Autologous bone continues to be the “gold standard” for bone regeneration, however their availability is limited and it involves a second surgery at the donor site which may lead to post-operative morbidity and patient discomfort [2].

Despite the large number of bone graft substitutes investigated in the past 40 years, none of them so far appears to be able to match the performance of autologous bone. The “ideal bone graft substitute” should be biocompatible, maintain a three-dimensional support during bone healing (osteoconductive), stimulate the bone growth (osteoinductive) and be gradually replaced by the newly formed bone [3-6]. The end objective being the full regeneration of the bone defect in the shorter time possible. Most common synthetic bone graft substitutes contain calcium phosphates, most of them hydroxyapatite (HAp), β -tricalcium phosphate (β -TCP) and their mixtures [7,8]. Fabrication of these materials usually involves sintering at high-temperatures which leads to materials that are chemically more stable,

with higher grain size and density, and lower porosity, pore size and surface area, when compared with calcium phosphates obtained by low-temperature processes. Altogether, these characteristics may reduce material bioactivity and osteoconductivity and prolong resorption time [3,9]. In contrast, nanostructured calcium phosphate biomaterials are closer to biological apatite than sintered materials, with physicochemical and morphological similarities to the mineral component of the bone. Nanometric calcium phosphates have shown enhanced osteoblast adhesion, proliferation and mineralization compared with microstructured materials leading to increased formation of new bone tissue within a short period [10,11]. Altogether, nanodimensional and nanocrystalline calcium phosphates represent a promising class of bone graft substitutes with improved biological and biomechanical properties.

Non-sintered calcium phosphates such as brushite (CaHPO₄·2H₂O) and monetite (CaHPO₄) are less frequently used clinically but there is increasing evidence of their potential in bone regeneration. Brushite in

***Corresponding author:** Sussette Padilla, AzureBio SL, C/Ronda de Poniente 16 L, 28760 Tres Cantos, Madrid, Spain, Tel: +34918031715; E-mail: spadilla@azurebio.com

Received June 27, 2015; **Accepted** August 26, 2015; **Published** October 01, 2015

Citation: Padilla S, García de Castro A, Garzón-Gutiérrez A, Benito L, Enciso S, et al. (2015) Novel Nanostructured Zn-substituted Monetite Based Biomaterial for Bone Regeneration. J Nanomed Nanotechnol 6: 325. doi:10.4172/2157-7439.1000325

Copyright: © 2015 Padilla S, et al. This is an open-access article distributed under the terms of the Creative Commons Attribution License, which permits unrestricted use, distribution, and reproduction in any medium, provided the original author and source are credited.

the form of *in situ* setting injectable cement pastes or preset granules has been shown to be effective in bone repair [12-14]. Its dehydrated solid form, monetite, has also been the focus of some attention in the last decade, demonstrating considerable efficacy in bone regeneration [13-17]. Brushite is usually obtained from calcium phosphate hydraulic cementing reactions and can then be easily converted to monetite by thermal treatment between 80 and 300°C. Brushite and monetite have higher solubility at physiological pH than apatites or β -TCP [18]. They have been shown to support osteoblastic cells adhesion, proliferation and differentiation [19] and to be osteoconductive and rapidly reabsorbed and osseointegrated when implanted in bone [13,16,20]. In spite of their chemical similarity, monetite has been reported to have a faster resorption rate than brushite [13,17,21]. This has been attributed to hindrance of resorption by re-precipitation of insoluble HAp on the surface of implanted brushite [12,13] by a process which does not appear to occur for monetite [13,22].

Calcium phosphates are recognized as being bioactive and osteoconductive since they bond directly and tightly to newly formed bone and facilitate bone growth on their surface. They are in themselves not generally regarded as osteoinductive, however calcium phosphates with the adequate topography, geometry, composition, interconnecting macroporosity and microporosity in the appropriate amount, and size can be osteoinductive, inducing the formation of bone at ectopic locations [23].

Biomaterials containing silicon have also been widely investigated for bone repair. Bioactive glasses (BG), generally including SiO_2 and CaO in their composition, have been shown to be osteoinductive without the need for specific structures. This osteoinductive capacity of BG has been associated to the release of ionic species resulting from their dissolution, mainly of Si and Ca, which have a local stimulatory effect on cells implicated in bone formation [24,25]. BG have also been found to directly bond to new bone and become well osteointegrated by a complex process involving the formation of a surface layer of hydrated silica gel followed by the formation of a nanocrystalline HAp surface layer which promotes the adhesion of osteoproducer cells [24].

Present work describes a new multicomponent biomaterial for bone regeneration designed to meet the criteria of an ideal bone graft substitute by serving as a temporary scaffold that provides with a local environment that favors bone formation until it is resorbed and replaced by new bone. Biomaterial incorporates hydrated silica gel in order to induce osteoinductive behavior and a combination of calcium phosphates, i.e: monetite, HAp, and amorphous calcium phosphate, to modulate its solubility profile. Zinc was also incorporated to the biomaterial as it has been reported to induce osteoblastogenesis, osteoblast mineralization and inhibit osteoclastic activity [25-31].

Materials and Methods

Experimental material

Biomaterial, Sil-Oss[®], was obtained by a proprietary method [32] involving a hydraulic acid-base cementing reaction carried out at room temperature that results in a solid that is subsequently crushed and sieved to a granule size between 0.25-1.0 mm.

Physical, chemical and microstructural characterization

Quantitative chemical analysis was performed by X-ray fluorescence in a MagiX Super Q Version 3.0 spectrometer (Philips Analytical) provided with an Rh X-ray tube and a power generator of 2.4 kW on fused pearls of the sample with spectral grade $\text{Li}_2\text{B}_4\text{O}_7$ (1:20).

Qualitative and quantitative phase analysis was performed by X-ray powder diffraction (XRD) using a D8 Advance (Bruker AXS) X-Ray diffractometer with LinxEye Super Speed Detector. The recording conditions were 10-70° (2 θ), step size 0.05° (2 θ), step time 1.05 s, $\lambda_{\text{CuK}\alpha 1}$ =1.54056 Å, V_a =40 kV and I_a =40 mA. In order to quantify crystalline and amorphous phases, pure α - Al_2O_3 (99.998 %, Fluka No. 06280), previously treated as elsewhere [33] was used as internal standard (10.00 wt. %). Quantification was performed using the Rietveld method [33] and GSAS-II software [34].

Parameters of monetite unit cell were refined using the software UnitCell from the Department of Earth Sciences at the University of Cambridge [35]. For refinement the angular position of ten selected diffraction peaks and their Miller index were employed. Only non-overlapping peaks were used and their angular positions were corrected with the aid of α - Al_2O_3 internal standard.

Transmission FTIR spectra were recorded in a Perkin Elmer Spectrum 100 spectrometer on pellets prepared mixing 1 mg of the samples and 250 mg of KBr (IR grade).

High resolution MAS-NMR spectra were carried out at room temperature in a Bruker Avance 400 spectrometer operating at 79.49 MHz (^{29}Si signal) and 161.98 (^{31}P signal). The powder sample was packed into a 4 mm \varnothing zirconia rotor and the spectra collected at a spinning rate of 10 kHz after $\pi/2$ irradiation pulse (5 and 6 μs for ^{29}Si and ^{31}P , respectively). The number of scans was 800 for silicon and 100 for phosphorous at 5 s intervals, in order to minimize saturation effects. External standards of tetramethylsilane ($\text{Si}(\text{CH}_3)_4$, TMS) and H_3PO_4 (85%) were used for measuring chemical shifts in ^{29}Si and ^{31}P , respectively. OriginPro 8.6 (OriginLab Corp.) software was used for deconvolution and analysis of spectra.

Specific surface area measurements were performed in a Monosorb Surface Area Analyser (MS-13, Quantachrome Instruments, USA) by N_2 adsorption at -196°C using the one-point BET method.

Open porosity, in the range 300 to 0.007 μm of pore diameter, was determined in a Hg-intrusion porosimeter (PoreMaster 33, Quantachrome Instruments, USA). The bulk density of the packed granulates was determined from their weight and volume. The apparent and real densities were determined by He picnometry (Multipycnometer, Quantachrome Instruments, USA) on the granulated sample and a powdered (< 45 μm) sample, respectively.

Surface and bulk microstructure of biomaterial granules were examined on graphite-coated samples using a field emission scanning electron microscope (FESEM; JSM6336F, JEOL USA Inc., USA) coupled with an X-Ray Energy Dispersive Analyzer (XEDS; Oxford X-Max, Oxford Instruments, UK). Cross-sections of the granules were prepared by embedding the granules in epoxy resin (EpoFix, Struers A/S) and cutting and polishing the blocks.

Nanostructure and composition was examined using a transmission electron microscope (TEM; JEM 2100, JEOL USA Inc., USA) equipped with X-Ray Energy Dispersive Spectroscopy microanalysis (XEDS, Oxford Instruments, UK). Samples were prepared by ultrasonic milling and dispersion in acetone prior to their transfer to holey carbon-coated copper grids.

In vitro testing

Solubility and ion release profile: Experiments were conducted in 0.1 M Tris-HCl buffer pH 7.40 at $37 \pm 1^\circ\text{C}$. Samples of ≈ 0.5000 g of the experimental granules (particle size 0.25 - 1.0 mm) were incubated in 200 ml of Tris-HCl at 1, 2, 5, 7 and 15 days. At the end of each incubation period

the resulting suspension was vacuum filtered through 0.2 µm-cellulose acetate membrane filter, and the solid residues quantitatively collected on the filter, dried at 80°C, and weighted to determine the solubility. The pH of the supernatant solutions was measured and the content of Ca, P, Si and Zn determined by Inductively Coupled Plasma Optical Emission Spectroscopy (ICP-OES; Iris Asvantage, Thermo Jarrell Ash, USA). The solubility of monetite granules of same size, also synthesized by a cementing reaction, and HAP were also studied for comparison.

Alamar blue cytotoxicity and proliferation test: To evaluate possible effects of dissolution products on osteoblast behavior, extracts of the biomaterial granulate were tested for cytotoxicity and cell proliferation. Extracts (0.1 g/mL) were prepared by incubation of the granulate in DMEM-F12 culture medium (DMEM-F12, Sigma D8437) supplemented with 1% of a 10UI/10 mg/ml penicillin/streptomycin solution (Sigma, P0781) (complete DMEM-F12) for 24 h at 37°C in an orbital shaker at 100 rpm. The resulting suspension was centrifuged at 350 g and filtered through a 0.22 µm filter. Filtrates were diluted and fetal bovine serum (FBS, Sigma, F7524) was added to a final concentration of 80% extract in 10 % FBS in complete DMEM-F12.

For the cytotoxicity assay, Human Osteoblast cells (HOb 406-05f, deposited at ECCAC by Cell Applications, Inc) were seeded in 96-well plates at a density of 50,000 cells/well in 100 µL/well of complete DMEM-F12 supplemented with 10% FBS (complete DMEM-F12/10%FBS) and incubated at 37°C in 5% CO₂ atmosphere. After 24 h, medium was replaced by biomaterial extracts, or controls, and incubated for further 24 h after which the media was replaced with 10% of Alamar Blue in complete DMEM-F12/10%FBS without phenol red and incubated for further 2 h at 37°C [36]. After incubation absorbance was measured at 570 nm using 620 nm as reference absorbance. Complete DMEM-F12/10% FBS was used as negative control. Complete DMEM-F12/10%FBS with 0.5 vol% Triton X-100 (Merck) was used as a positive control for cytotoxicity.

Same conditions as above were used for the determination of cell proliferation where DMEM-F12 /10% FBS was used as positive control. Viable cell numbers and cell morphology were studied after 1, 3 and 7 days.

Six replicas of each condition and time were analyzed for both assays. Significant differences between groups were established by the t-Student test (p<0.05).

In vivo assessment

A critical size defect in spongy bone in sheep [37] was used as a model to assess *in vivo* behavior of the biomaterial. The protocol was approved by the ethical committee of Centro de Cirugía de Mínima Invasión Jesús Usón (Cáceres, Spain) following the European Union guidelines for decreasing pain and suffering of animals.

Surgical interventions of the adult female Merino sheep (4 years old; 51±10 kg) were performed under aseptic conditions. General anesthesia was induced by isoflurane (minimal alveolar concentration=1; EtIso: 1.58). Intraoperative analgesia was maintained by intravenous injection of buprenorphine (0.01 mg/kg) and carprofen (4 mg/kg). Bilateral cylindrical holes (8 mm in diameter and 13 mm in depth) were drilled in the proximal tibia epiphysis, medial epicondyle of the femur and greater tuberosity of the humerus, under continuous irrigation with cold sterile saline. Debris were completely removed from the bone cavity by washing with sterile saline and excess fluid removed with a gauze before being filled with biomaterial granules. In case of bleeding, Espongostan® (Nycomed Pharma, Norway) was

used and retrieved after two minutes. Nine cavities were filled with the material and five empty defects used as control. Defects were covered by a fast resorbable collagen membrane (RCT Collagen tape; ACE Surgical Supply Co., USA) to prevent initial migration of the granules. Subcutaneous tissue and skin were closed with a resorbable suture. Postoperative analgesia was administered for 3 days by intramuscular injection of buprenorphine at 0.01 mg/kg/12 h. Anti-inflammatory Carprofen, at 2 mg/kg/12 h, and antibiotic Ceftiofur, at 1 mg/kg/24 h, were administered intramuscularly for 7 days. After 16 weeks, animals were euthanized under general anesthesia with a potassium chloride intravenous injection.

Following sacrifice, bone sections containing the implants and controls were removed and processed for histological evaluation without decalcification. Specimens were fixed in 4 vol% formal saline and dehydrated using incremental grades of ethanol from 70 to 100%. Bone samples were thereafter infiltrated, embedded and polymerized in polymethylmethacrylate resin. Sections of 5 µm in thickness were stained using Goldner's trichrome and Von-Kossa's techniques for histological examination. Histomorphometric analysis was carried out on longitudinal histology sections at the center of the defect. Percentages of new bone (%NB) including mineralized bone and osteoid, connective tissue (%CT), bone marrow, and residual material (%RM) were calculated against the area occupied by the initial defect. Percentage of material resorption (%R) was determined according to equation 1 where %IGV corresponds to the percentage of the defect area occupied by granulates at implantation. Direct estimation of granulate area and %IGV upon implantation was carried out on cylinders with the same size of the created defects (8 mm in diameter and 13 mm in deep) filled with granulate biomaterial and embedded and polymerized in polymethylmethacrylate resin and cut into longitudinal sections. ImageJ software was used for the histomorphometric study.

$$\%R = 100 - \frac{\%RM * 100}{\%IGV} \quad (1)$$

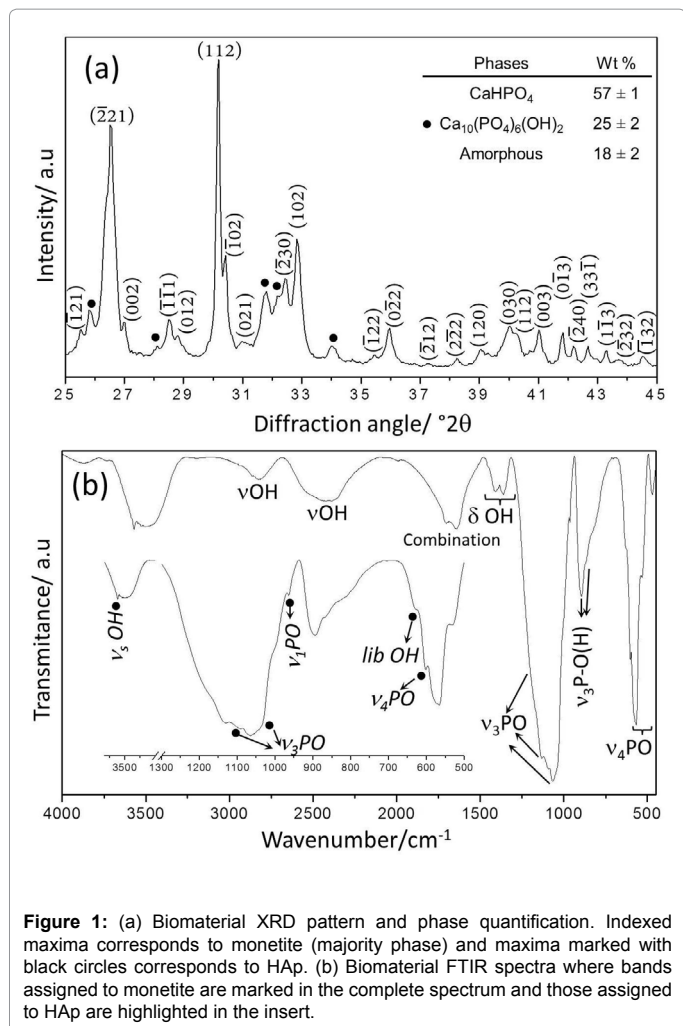
Results

Chemical and physical characterization

Qualitative phase analysis on the XRD pattern of the biomaterial showed monetite, (CaHPO₄, JCPDS No. 09-0080), as major crystalline phase, and maxima corresponding to HAP (JCPDS No. 9-0432) (Figure 1a). No maxima assignable to other crystalline phases were detected. Quantitative phase analysis revealed a composition of 57 wt % of monetite, 25 wt % of HAP and 18 wt % of an amorphous phase.

The infrared spectrum (Figure 1b), revealed the presence of bands corresponding to monetite [38] and hydroxyapatite [39]. The following bands were assigned to monetite: OH stretching at 2828 and 2400 cm⁻¹, PO stretching (ν₃) at 1170,1127 and 1067 cm⁻¹, ν₁ at 1000 cm⁻¹, ν₃ P-OH at 898 and 868 cm⁻¹, P-O bending (ν₄) at 569 and 534 cm⁻¹, combination at 473 cm⁻¹ P-O bending (ν₂) at 435 and 408 cm⁻¹ and OH in-plane bending at 1409 and 1359 cm⁻¹. Bands at 1703 and 1638 cm⁻¹ appeared to correspond to a combination of P-O vibration with possible influence of OH groups. Remaining bands correspond to HAP: PO stretching (ν₃) at 1094 and 1030 cm⁻¹, ν₁ at 962 cm⁻¹, ν₄ at 604 cm⁻¹ and OH bands at 3570 cm⁻¹ (ν_s) and 631 cm⁻¹ (librational mode). No bands attributable to the silicate group could be detected due to their overlap with phosphate bands [40].

The presence of Zn and Si was confirmed by the results of chemical analysis (Table 1). Zn was found to be present in the material in a 1.1 wt% and silicon in a 2.5 wt%. The ³¹P and ²⁹Si MAS-NMR



spectra of material are shown in Figure 2a and 2b, respectively. The ³¹P spectrum exhibited (Figure 2a) three signals at chemical shifts of -1.54, -0.33 (shoulder) and 2.72 ppm. The first two signals originate from the two different kind of P atoms in the triclinic monetite unit cell (Space Group P -1) [41,42]. The broadening and overlapping of the two peaks indicated low crystallinity. The third signal, at 2.72 ppm, was attributed to the single P atom in the hexagonal crystalline network of hydroxyapatite [43]. Although the NMR response from a well-ordered hydroxyapatite structure should feature a narrow peak, some broadness causing partial overlap with adjacent monetite peaks was observed and attributed to the presence of amorphous calcium phosphate with a characteristic very broad ³¹P NMR signal at the same chemical shift than the well-ordered crystalline hydroxyapatite [44]. Signals corresponding to Si resonances (Figure 2b) appear even wider than those of P, indicating that Si atoms are within an amorphous chemical surrounding as would correspond to hydrated silica gel. Two different chemical environments were identified for the Si atoms, at -111.6 and -101.8 ppm. They were attributed to Q₄ and Q₃ silicon types, respectively, where Q_n denotes a SiO₄ tetrahedron connected to n other SiO₄ tetrahedrons in an amorphous network [45]. The relative amounts of Q₄ and Q₃, as estimated from the areas of their deconvoluted signals, were 64 and 36%, respectively. A certain amount of network modifiers, Ca, or H, could be associated to Q₃ silicon tetrahedrons according to previously published results on the structure of hydrated silica gels of similar origin [46].

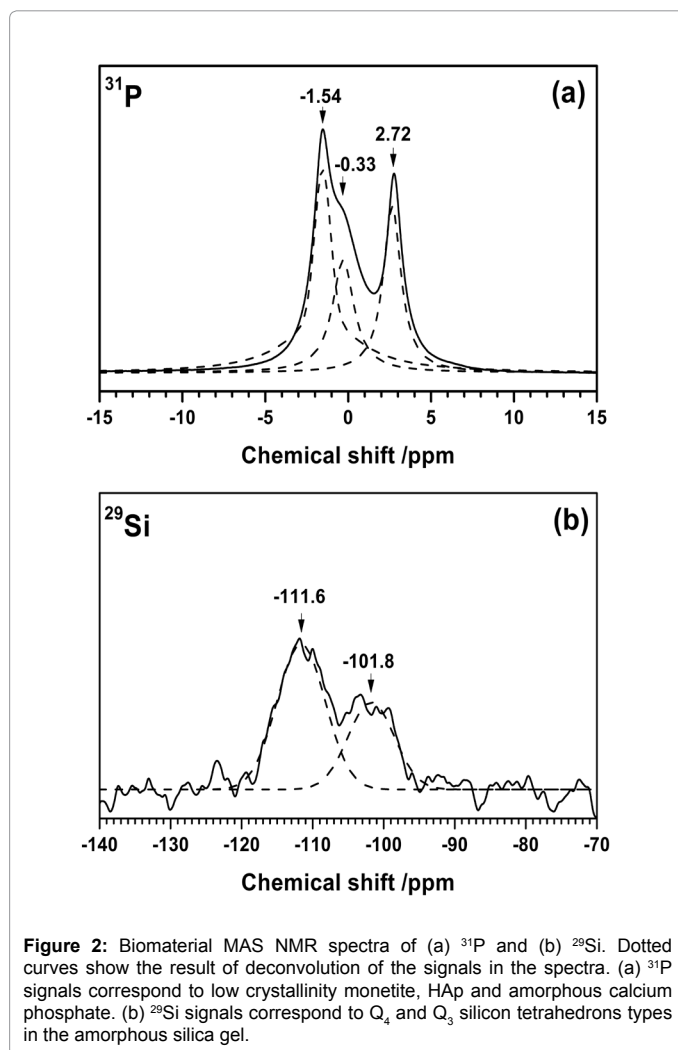
	CaO	P ₂ O ₅	SiO ₂	ZnO	L.O.I
Weight ± CI %	42.2 ± 0.3	44.4 ± 0.3	5.60 ± 0.05	1.36 ± 0.05	6.4 ± 0.1

CI: Confidence interval; n=3; α=0.05; L.O.I.: Lost on ignition at 1000°C.

Table 1: Chemical composition of the material determined by X-ray fluorescence.

Following the NMR and DRX analysis, silicon in the biomaterial was found to be only present as an amorphous phase. Thus, from the SiO₂ content, the amount of hydrated silica gel ([SiO₂·H₂O]_n) [46] was estimated to be 6.8 wt% and the difference with the total amount of amorphous phase in biomaterial (18 wt%) was assigned to amorphous calcium phosphate (11 wt%).

Incorporation of Zn in the monetite lattice was investigated by XRD comparing the unit cell parameters and crystal domain size of the triclinic (Ca,Zn)HPO₄ with a biomaterial obtained by the same procedure but without Zn (CaHPO₄). Data in Table 2, indicate that the incorporation of Zn caused shrinkage in the parameters and volume of the cell unit of the triclinic monetite. The addition of Zn also reduced significantly the crystal domain size compared with the material without Zn. These results confirmed the incorporation of Zn into the structure of the monetite present in the biomaterial. Assuming that all the Zn in the biomaterial is associated to crystalline monetite, the estimated degree of substitution of Ca for Zn in the monetite network, resulting



Unit cell parameter	CaHPO ₄	(Ca,Zn)HPO ₄
a (Å)	6.8920 ± 0.0008	6.8746 ± 0.0009
b (Å)	6.5429 ± 0.0007	6.5318 ± 0.0008
c (Å)	7.0054 ± 0.0006	6.9864 ± 0.0006
α (°)	96.238 ± 0.008	96.214 ± 0.009
β (°)	103.843 ± 0.008	103.786 ± 0.009
γ (°)	88.314 ± 0.009	88.40 ± 0.01
Cell Volume (Å ³)	304.91 ± 0.04	302.89 ± 0.04
Crystal domain size (nm)	421 ± 70	105 ± 31

±: confidence interval; n=3; α=0.05

Table 2: Effect of zinc addition on the unit cell parameters and crystal domain size of crystalline CaHPO₄

from the quantitative phase and chemical analysis, was 4 atom%.

Granules of biomaterial have irregular shapes (Figure 3a and 3b) with smooth edges and a rough and porous surface (Figure 3a-d). Surface of the granules is formed by homogeneously distributed rounded agglomerates of similar morphology with an average size of 3.3 μm (Figure 3c and 3d). These agglomerates provide microporosity and rugosity that is randomly and homogeneously distributed throughout the surface and inside material. These micropores (<10 μm) ranged between 0.15 and 3.5 μm with an average size of 1.8 μm (Figure 3d). SEM (Figure 3c-3e) also revealed presence of macropores (>50 μm) and mesopores (50-10 μm) both superficially and inside of granulates ranging between 15 to 215 μm, being larger at the surface (average size 53 μm) than inside of granulates (average size 25 μm).

Pore size distribution of granules obtained by Hg porosimetry is displayed in Figure 3f. Pores larger than 50 μm were assigned to intergranular spaces between neighboring granules of the packed material. The remaining pores, smaller than 10 μm, were assigned to open intragranular porosity inside the granules. These pores showed two maxima center at 1 μm and 20 nm. This intragranular pore size observed by Hg porosimetry corresponds to the size of the interconnections between the larger inner pores observed by SEM (Figure 3c-e).

Coincidence of the density of the granulates (2.821 g/ml) and the equivalent powdered material (2.828 g/ml) indicated that all the porosity within the biomaterial was open.

Altogether, according to Hg porosimetry and the bulk density of the granulates (0.5 g/mL), the total porosity of packed granules was as high as 82 vol%, of which 32 vol% corresponded to the intergranular space and 50 vol% to intragranular porosity. Packed biomaterial granulates could therefore be defined as having (i) spaces of about 200 μm formed between packed granules, (ii) pores at surface and inside granules with diameters ranging 6 nm to 215 μm with interconnections between 6 nm and 3 μm.

The material showed a high specific surface area (79 ± 1 m²/g), which was consistent with the rough morphology and porous structure observed by SEM and Hg porosimetry.

EDS analysis of the biomaterial showed a homogeneous distribution of elements Ca, P, Si, Zn, both on the surface and inside of the granulates (representative EDS spectrum of an area of the material is showed in the inset of Figure 4a. Some differences in the ratio of elements were observed when spot spectra were taken on different points of the same area. Nevertheless, even at 40k magnification (Figure 5a and 5b), no specific morphology or composition could be attributed to any of the crystalline or amorphous phases previously identified. Transmission

electron micrographs (Figures 5c and 5d) revealed a nanometric structure of the biomaterial composed of different shape nanosized particles. Rounded particles (≈3 nm) were Si-rich and attributed to amorphous silica gel. Nanorod shaped particles, smaller than 160 nm and with average particle size of 50 nm, were found to be rich in Ca and P.

In vitro solubility

The solubility profiles of biomaterial, HAp, and monetite granules are displayed in Figure 5a. Dissolution of biomaterial was evident from the first day of incubation in Tris-HCl buffer, when the concentration of dissolved material reached 145 mg/L (Figure 5a). The dissolution of material increased over time reaching 475 mg/L after 15 days (Figure 5a). The solubility of the biomaterial and monetite were similar during the first 2 days. However, after 15 days solubility of the biomaterial was found to significantly exceed that of monetite (330 mg/L). Solubility of HAp in the same period was very low reaching only 15 mg/L. The pH of the dissolution medium did not vary greatly over time, maintaining values between 7.4 and 7.7.

Release profiles of Ca, P, Si, and Zn species during dissolution of the biomaterial in Tris-HCl buffer are shown in (Figure 5b). Concentrations of Ca, P, Si, and Zn rapidly increased during the first day of incubation. Increase in concentration slowed down thereafter but continued until the end of the observation period for P and Si, whereas the calcium concentration drastically dropped at day 15. After the initial increase at day 1, Zn concentration dropped slightly until the end of the observation period. The molar ratios between dissolved elements along the whole study period differed largely from the ratios found for the biomaterial, which indicated that the dissolution of the biomaterial is incongruent. Moreover, the drop of Ca and Zn concentrations observed after the seventh and first day, respectively, indicated that a Ca- and Zn- consuming process was also taking place. This process most likely involves the precipitation of a calcium phosphate with a Ca/P rate higher than that found in the dissolved biomaterial components.

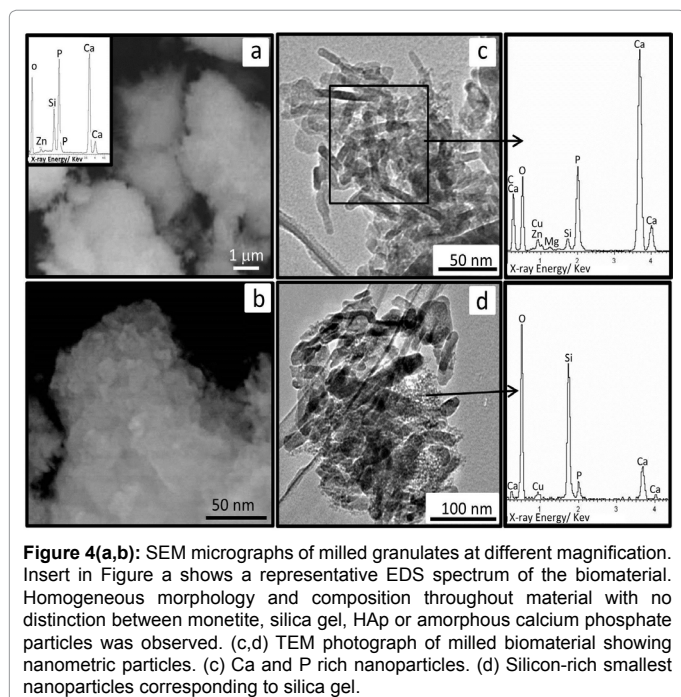
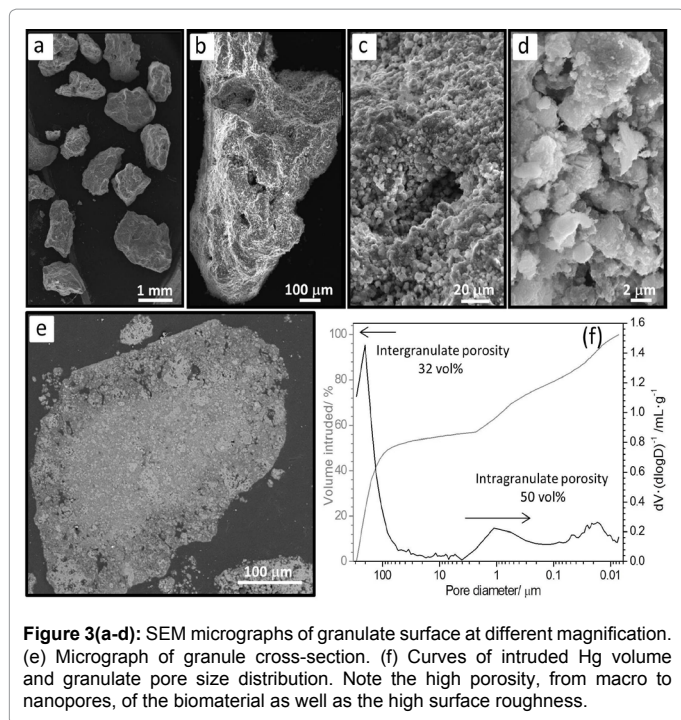
In vitro proliferation and cytotoxicity

No significantly differences in proliferation of HOb cells in the presence of biomaterial extract were observed when compared to control cultures (Figure 6a). HOb cells showed an elongated morphology with no apparent difference between controls and cells exposed to biomaterial extracts (Figure 6b-6c). Cytotoxicity of the biomaterial extract at 80 vol% in HOb cells was 5 ± 4% against 96 ± 3% observed for the positive control (Triton X-100). Biomaterial was therefore determined to be non-cytotoxic.

In vivo evaluation

Empty osseous defects used as control showed partial regeneration, with only 53 ± 14% of the defect regenerated, after 16 weeks of implantation (Figure 7a) as expected for critically-sized defects. Histological evaluation of control defects showed a homogenous tissue response with partial regeneration and adipose tissue developed throughout the non-regenerated space. Neither hematopoietic bone marrow nor connective tissues were found in any of the control defects in which the limited new bone formed inwards from the border of the defects. In two out of the five cases, cortical bone was formed at the superficial part of the defect with the remaining non-regenerated area forming a cavity under the cortical.

Table 3 shows results of the histomorphometric analysis after 16



weeks. Volume of the defects implanted with biomaterial was restored at $89 \pm 9\%$ of the original defect showing an advanced stage of bone regeneration after 16 weeks (Figure 7b). The remaining 11% was filled with loose connective tissue without detectable presence of biomaterial.

New trabecular bone was formed throughout the cavity, filling it and reaching the cortical where cancellous bone was formed. New trabecular bone showed disorganized, wide and anastomosed trabeculae and a great osteogenic activity (Figure 7b and 8a). Newly formed trabeculae were estimated to occupy $35 \pm 6\%$ of the initial defect.

Intense osteogenic activity was evidenced by large fronts of active osteoblasts on the surface of newly formed trabeculae and wide osteoid lines formed by deposition of bone organic matrix (Figure 8b and 8d). Regenerated bone was mostly mineralized with the exception of few non mineralized areas (Figure 8c). In addition, vascular cavities surrounded by osteoid lines were observed in the new trabecular bone (Figure 8a and 8d). Newly formed bone showed healthy vascularized adipose and hematopoietic bone marrow (Figure 8d).

Identified remaining biomaterial granules showed clear signs of resorption throughout the granules that appeared mostly as smaller fragments (Figure 8a,c,d). Initial average area of biomaterial granulate was 0.148 mm^2 which after 16 weeks was found to have decreased to 0.048 mm^2 , which represents a $67 \pm 8\%$ reduction in size of the originally implanted granules. Reduction in granule size was associated to a reduction of total area occupied by remaining material which was found to have reduced from $\%IGV = 68 \pm 3\%$ to $\%RM = 10 \pm 5\%$, indicating $85 \pm 7\%$ of biomaterial resorption (%R).

Osteogenic cellular activity and bone formation was not only seen around granulates but also inside the fragments of remaining biomaterial (Figure 8c and 8d). Almost all the area of residual biomaterial was found completely osteointegrated in the newly formed trabecular bone matrix. Areas of the biomaterial not covered by bone trabeculae were in direct contact with bone marrow and seen to be surrounded by osteoclasts (Figure 8d) and other multinucleated cells in the process of resorption. Osteoclasts were also observed on the surface of the new formed bone suggesting that bone remodeling, typical of normal mature bone, was taking place. Altogether, intense cellular activity and evidence of bone remodeling support the finding that after 16 weeks fully functional mature bone had almost completely replaced the implanted biomaterial granules (Figure 8d). No adverse reactions were observed.

Discussion

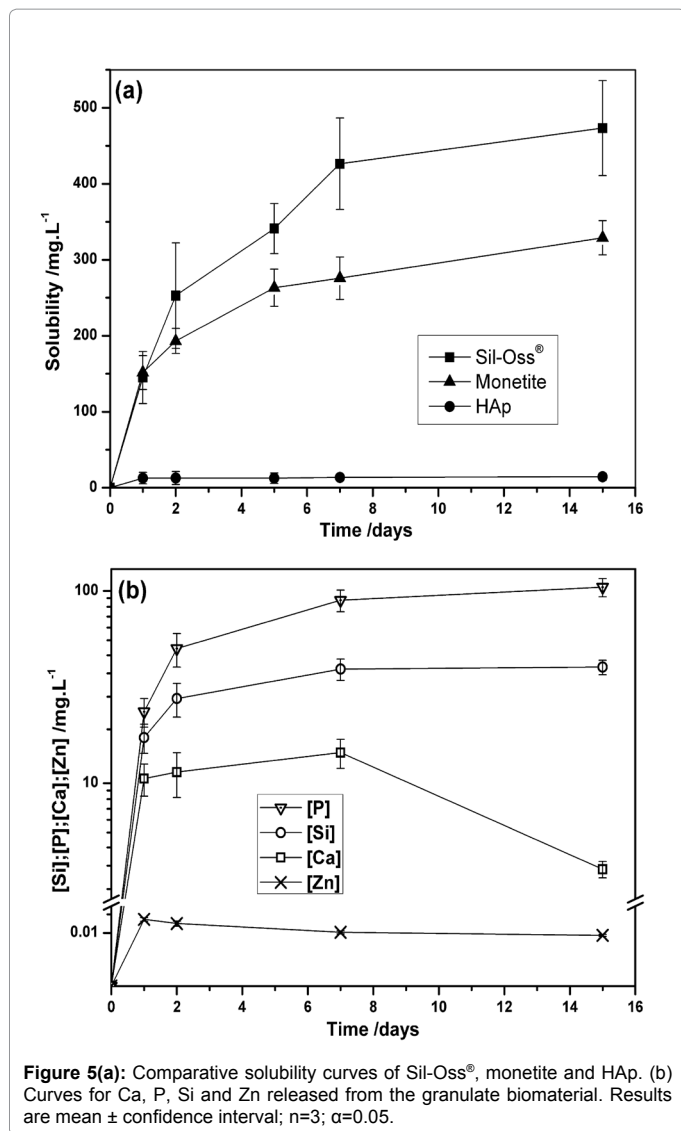
Biomaterial was designed to release ionic species with stimulatory effects for bone regeneration while acting as a temporary scaffold to support bone growth. This novel biomaterial combines Zn-substituted monetite (57 wt%), hydroxyapatite (25 wt%), amorphous calcium phosphate (11 wt%) and hydrated silica gel (7 wt%). The partial substitution of 4 atom% of Ca for Zn in the monetite lattice was demonstrated by the decrease in the parameters and volume of the cell unit and crystal domain size of the monetite phase as a result of the lower ionic radii of Zn^{2+} (0.74 \AA) compared with Ca^{2+} (0.99 \AA). To the best of our knowledge there are no precedents reporting a material with a similar composition, neither substitution of Ca^{2+} in monetite by other ions and specifically by Zn^{2+} .

The biomaterial presented a homogeneous and intimate distribution of its different components of nanometric size. As previously reported, this is an important feature over microstructured

	%RM	%NB	%NBM	%NBM+RM	%CT	%R	%ARRM
Sil-Oss®	$10 \pm 5\%$	$35 \pm 6\%$	$80 \pm 8\%$	$89 \pm 9\%$	$11 \pm 9\%$	86 ± 7	67 ± 8

%RM: percentage of remaining material
 %NB: percentage of new bone including mineralized bone and osteoid
 %NBM: percentage of new bone matrix including NB and bone marrow
 %NBM+RM: percentage of defect filled with new bone matrix and remaining material
 %CT: percentage of connective tissue.
 %R: percentage of material resorption
 %ARRM: percentage of average granule area reduction
 ±: confidence interval; n=9; $\alpha=0.05$

Table 3: Results of the histomorphometric analysis after 16 weeks.



materials, as nanometric morphology contributes to increased reactivity of the material, improved protein adsorption and interaction with osteoblasts, as well as facilitating biomaterial resorption by dissolution and by osteoclast and macrophage activity [9-11,47,48].

In addition to composition and morphology, the biomaterial also showed relevant features that contribute to the biological performance of a bone regeneration material such as high interconnected porosity, specific surface area and surface roughness.

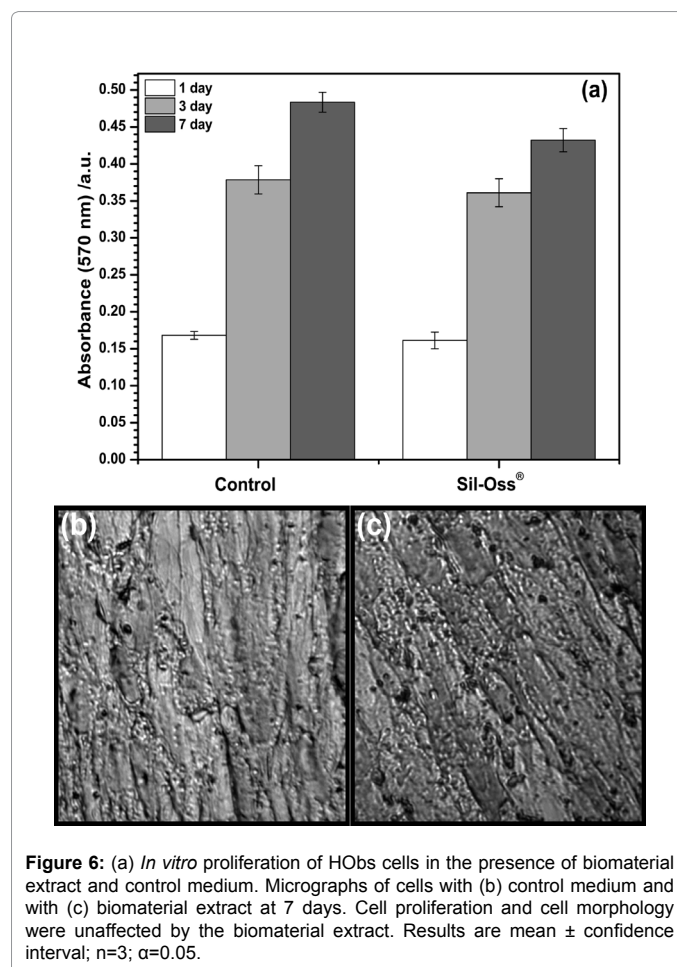
Porosity is acknowledged to play a crucial role in bone regeneration by enhancing osteogenesis [49]. In granulate materials, the intergranular spaces of the packed granulates provide with an interconnected macroporosity ($\approx 200 \mu\text{m}$) that allows for osteoconduction, vascularization and formation of new bone around the granules. Biomaterial also shows high intragranular interconnected (50%) macro ($<50 \mu\text{m}$), meso ($50\text{-}10 \mu\text{m}$), micro ($10 \mu\text{m}\text{-}100 \text{nm}$) and nanoporosity ($>100 \text{nm}$). This high interconnected porosity and pore dimensions (from macro to nanopores) are important for the effective inwards diffusion of nutrients and release of biomaterial dissolution products (e.g. Ca, P, Si, Zn ionic species), and also favor material

resorption [49]. Macropores also facilitate cellular colonization and vascularization inside the biomaterial. Microporosity is also essential, allowing for immediate protein and cell adhesion, cell migration and osteointegration [49,50] and also providing with an important space for bone ingrowths [51]. Micro and nanopores also play an important role in the osteoinductive potential of the materials [52].

The high porosity of the biomaterial, its high surface roughness and nanometric size of its components result in a specific surface area that is up to 40 times higher than reported for monetite or brushite cements with micro size crystals ($79 \text{ m}^2/\text{g}$ vs $2\text{-}4 \text{ m}^2/\text{g}$) [14,17]. Larger surface areas contribute to higher bone inducing protein adsorption as well as higher ion exchange [53] and increased interaction with cells [54]. High surface roughness is also reported to enhance attachment, proliferation and differentiation of anchorage dependent bone forming cells [53].

Solubility of the biomaterial was found to be higher (475 mg/L) than monetite alone (330 mg/L), after 15 days in Tris-HCl buffer, and much higher than synthetic HAp (15 mg/L). The reported solubility of the different components of the biomaterial at 25°C is, silica gel (125 mg/L) > monetite (48 mg/L) > amorphous calcium phosphate (1.2 mg/L) > HAp (0.3 mg/L) [18]. Assuming that the solubility ratio between the different components of the biomaterial does not change in the experimental conditions used hereby, it can be expected that silica gel and Zn-substituted monetite will dissolve faster than the amorphous calcium phosphate and HAp.

According to the release profiles of Ca, P, Si and Zn, the dissolution



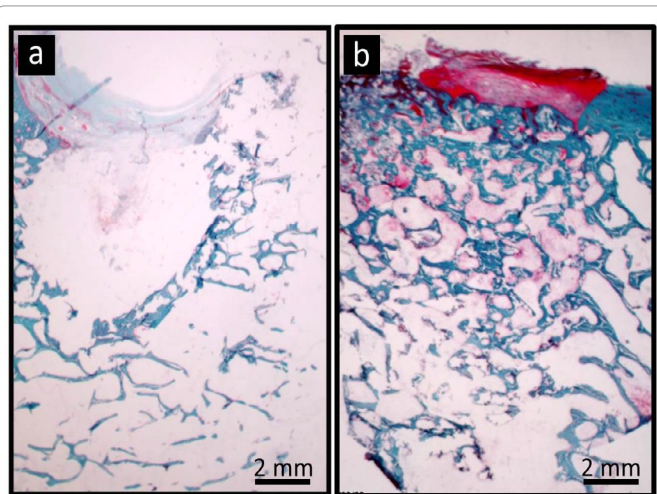


Figure 7: Representative low magnification histological images of critical size defects in sheep after 16 weeks (a) with no implanted material and (b) treated with biomaterial, showing significantly greater bone regeneration of the treated defect when compared to untreated control. Goldner's trichrome stain shows mineralized bone in blue, collagen fibers present in non-mineralized tissue in red, corresponding to connective tissue outside defect and to non-mineralized organic bone matrix (osteoid) inside defect.

of biomaterial is incongruent and appears to take place by three overlapping processes. The fastest of them would correspond to the dissolution of the more soluble phases, hydrated silica gel and Zn-substituted monetite, and would account for the fast increase in the concentration of Si, Ca, P and Zn. A second process, slower than the former, would be the dissolution of amorphous calcium phosphate and HAp, which would provide with additional Ca and P to the surrounding media. A third process would involve the precipitation of a Zn-containing apatite-like calcium phosphate, with a Ca/P ratio higher than in the dissolution media, resulting in a decrease in Ca, and Zn concentrations. However further dissolution studies including kinetics and analysis of residual material should be conducted to confirm the above considerations.

Ca, P, Si and Zn ions released from the biomaterial are known to trigger intracellular responses activating key mechanisms leading to enhanced new bone growth [25,27,28]. Silicon is known to be an essential element for metabolic processes associated with bone growth [55] and calcification of bone tissues [56]. Silicon, through the formation of an amorphous silica gel, has also been reported to favor local precipitation of apatite on the surface of implanted Si-containing biomaterials and in this way improve the bond with the adjacent newly formed bone [55,57]. Similarly, calcium ions have been shown to play an important role in bone remodeling and favor osteoblast proliferation, differentiation and extracellular matrix mineralization [58-60]. Release of Ca and Si by dissolution has been associated to the osteoinductive effect of BG [24,25], and to enhance osteogenesis by regulating osteoblast proliferation, differentiation, and gene expression [25,61] and promote angiogenesis [25,62].

Inorganic phosphate is also crucial for bone growth and mineralization [63,64] with dietary deficit leading to diseases like rickets and osteomalacia (undermineralized soft bones) [64]. Inorganic phosphate has been shown to modify gene expression during osteoblast differentiation [65,66] and to enhance the bioactivity of glasses and glass ceramics [67].

Zinc accumulates preferentially in bone [68] where it has been found to play an essential role in growth and skeletal development [26,69]. Incorporation of Zn into biomaterials has been found to stimulate osteoblast differentiation by up-regulating the expression of bone marker genes such as alkaline phosphatase (ALP), collagen type I (Col-I), osteocalcin (OCN), and osteopontin (OPN), and further promoting extracellular matrix mineralization via increased collagen secretion and calcium deposition [25-30]. There is also evidence that Zn inhibits osteoclastic activity [30,31]. Incorporation of Zn in a brushite cement, estimated at 1 wt%, has been previously reported to have a stimulatory effect in bone formation in pig bone defects when compared to carbonated apatite cement with no Zn [70]. A report of HAp and HAp/TCP substituted by Zn implanted in rabbit femoral model for bone regeneration suggests an optimum amount of Zn of 0.32 wt% [71] while another study in rabbits on zinc-containing α -TCP suggest that 0.03 wt% of Zn may be optimum for promoting bone formation without inflammation [72]. There is therefore no clear consensus as to what the appropriate levels of Zn should be for a bone regeneration material and the rapid metabolism of rabbits and differences in biomaterials and experimental conditions may be providing misleading information as to the optimum amounts of Zn. Histology of the critical defects implanted with the present biomaterial did not reveal undesirable adverse inflammatory effects and therefore the 1.1 wt% of Zn contained in the present biomaterial does not appear to be in excess. The maximum concentration of Zn found in

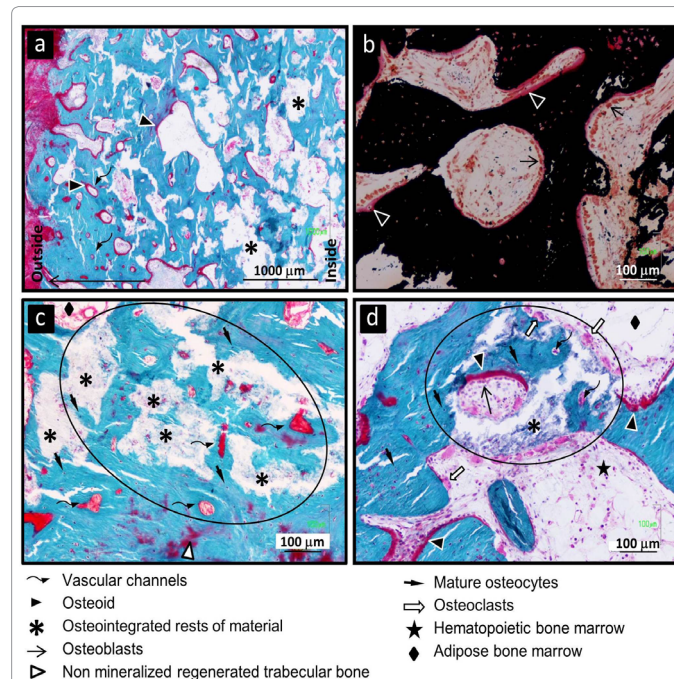


Figure 8: Histological images of defects implanted with biomaterial showing an advanced stage of bone regeneration. (a) Well-mineralized regenerated trabecular bone (blue) with osteogenic activity and vascular channel systems surrounded by osteoid lines (red). (b) Cubic active osteoblasts associated to wide osteoid lines at well mineralized trabecular bone surface. (c, d) Circular areas showing osteointegrated remains of partially resorbed granulates surrounded by mineralized bone with vascular channels and osteocytes. (d) Remodelation of new bone by osteoclast and resorption of osteointegrated granulates by osteoclast at their bone-free surface in contact with bone marrow. (a, c, d) Stained with Goldner's trichrome technique showing mineralized bone in blue and collagen fibers present in non-mineralized tissue in red, corresponding to connective tissue outside defect and to non-mineralized organic bone matrix (osteoid) inside defect. (b) Stained with Von Kossa showing mineralized bone in black and non-mineralized organic bone matrix (osteoid) in red.

the medium during the dissolution of 0.5 g of the biomaterial was 0.03 mg/L, corresponding to 8 µg of Zn and representing a 0.15 wt% of the total Zn contained in the biomaterial. It should be noted that the recommended daily intake for Zn is 7.5 to 16.3 mg/day [73] which assuming oral bioavailability of 30% is three orders of magnitude above that released from the biomaterial and should therefore be of no health concern in its clinical use.

In vitro osteoblast cell cultures resulted in lack of toxicity and no apparent changes in morphology. Further work is warranted as to determine the role and contribution that the biomaterial components and Ca, P, Si and Zn ions released may have on biological performance.

In vivo evaluation demonstrated the efficacy of the material in the restoration of volume in critical bone defects. Defects were found to be at an advanced stage of regeneration with active bone remodeling, formation of mineralized trabecular bone and remarkable osteogenic activity and high degree of vascularization. After 16 weeks implanted granules appeared fragmented and reduced in size and remains were found to be well osteointegrated in the newly formed bone matrix and to have been colonized by cells and new bone.

It is generally acknowledged that *in vivo* performance of bone graft biomaterials is determined by a combination of physical, chemical and biological factors. Physical factors include surface area, porosity and pore size, and crystal parameters like crystal size, crystal imperfections, and grain size. Chemical factors relate to composition and ionic substitutions in the material. Biological factors include affinity of cells and proteins for the biomaterial as well as its capacity for intimate bone contact and the biological models used in their evaluation. An ideal bone regeneration biomaterial should also be resorbable, thus providing with a temporary osteoconductive scaffold that is gradually replaced by new bone. Resorption is most often associated to two simultaneous processes, dissolution and cell mediated. Again, these processes are also greatly influenced by material physicochemical characteristics, including solubility, pore structure, surface area and crystallinity.

Present biomaterial has been tailored in composition to be gradually resorbed and stimulate the bone formation at the same time that it is replaced by new bone. Composition resulted from a novel combination Zn-monetite, hydroxyapatite, silica gel and amorphous calcium phosphate. Material was found to be nanostructured, with high specific surface area, porosity and roughness. The advantageous physical properties of the obtained biomaterial are related to the synthesis method of the biomaterial which involves a hydraulic cementing reaction in which material consolidation is achieved through a low-temperature dissolution-precipitation process. Hydraulic cementing reactions result in hydrated compounds with morphologies and compositions very similar to the calcium phosphates found in the mineralized tissues, with high specific surface area, porosity, surface roughness and nanostructure [74]. Nanometric morphology of the present biomaterial appears to be related to the use of nanometric reactants and incorporation of Zn.

Present biomaterial shows significant differences when compared with widely used commercial bone graft materials such as anorganic xenograft HAp, synthetic HAp, β-TCP and bioactive glasses. Xenograft HAp, are reported as providing an effective osteoconductive support for restoration of bone volume but being very slowly resorbed [75] or non-resorbed [76]. On the other hand, synthetic bone graft materials such as HAp, silicon-substituted HAp, β-TCP and their mixtures are most often sintered during manufacture. Sintering results in reduced

open porosity, low surface area, and high crystallinity and density, all of which are detrimental to their surface reactivity, *in vivo* biodegradation and osteointegration [9]. BG are also obtained by high temperature fusion but, although they induce bone formation and have shown better biological performance than calcium phosphate ceramics [77], their use has been limited because they cannot effectively be made into porous scaffolds without crystallization during sintering [78]. BG have shown very different resorption rates depending on their composition and granulate size. For example, Bioglass 45S5 particles smaller than 300 µm are likely to become empty HAp shells within 4 weeks, whereas S53P4 glass particles of 1-4 mm can still be found 14 after years implantation [78]. Resorption of BG has been seen to be mainly due to solution-mediated dissolution rather by cellular activity.

Materials closer the present biomaterial in their physicochemical characteristics include calcium phosphate cements such as HAp and brushite cements. Both materials have been evaluated *in vivo* in a similar critical defect model in sheep that allows for a direct comparison [79]. Resorption speed was reported to be very different for brushite and apatite cements, with 74% remaining apatite and ≈24% remaining brushite cement after four months. In the same time period, new bone matrix, defined as trabecular and intertrabecular space, was reported to be 15% for apatite and ≈40% for brushite cement. Comparatively, the % of remaining material for Sil-Oss® was found to be lower, 10%, and the % of bone matrix (NBM) occupying the critical defect was significantly higher at 80%. In addition, new bone formed in the defects filled with brushite after 4 months showed woven trabeculae associated with immature bone while defects treated with present biomaterial presented a mature bone structure involved in active bone remodeling. Increased resorption and increased bone formation observed for present biomaterial is likely to be a consequence of biomaterial composition as well as the increased porosity provided by a granular structure when compared to the monolith resulting from the injection of cement. Cellular involvement is commonly reported in the resorption of calcium phosphates. Macrophages have been reported to be mainly responsible in cell-mediated resorption of brushite and monetite while osteoclasts are more often associated to resorption of apatite [13,79]. Cell-mediated resorption of present biomaterial was found to involve osteoclast and other multinucleated cells.

Altogether, this novel combination of various calcium phosphates with different resorption rates in combination with silica gel and with Zn have shown a high biological performance compared with other bone graft materials. A sequential resorption of the material is proposed in which the more soluble components, silica gel and Zn-substituted monetite dissolve faster than amorphous calcium phosphate and HAp which continue providing long-term support for bone growth until complete regeneration of the defect. Maintenance of volume suggests that biomaterial appears to reach a compromise between resorption and bone formation thus providing with an effective temporary scaffold that provides a sustained release of Ca, P, Si and Zn ionic species which have a stimulatory effect of bone growth.

Conclusion

A new nanostructured bone regeneration biomaterial was obtained consisting of a novel combination of Zn-substituted monetite, hydroxyapatite, amorphous calcium phosphate and hydrated silica gel. Physical and chemical characterization of the biomaterial demonstrated a homogenous nanometric structure with high interconnected porosity from macro to nanopores, high roughness and high surface area. Different solubility of its components provides a gradual dissolution of

the biomaterial releasing Ca, P, Si and Zn which are known to have a stimulatory effect on bone growth.

The biomaterial was found to effectively restore bone volume and regenerate the defect and at the same time it showed significant resorption and replacement by new active bone. Newly formed bone was mature with high degree of vascularization and abundant osteogenic activity. Therefore, biomaterial was found to meet the design criteria of acting like a temporary scaffold for bone growth, gradually being replaced by the new formed bone and releasing inorganic ionic species likely to have a stimulatory effect for bone growth. This material has chemical and physical characteristics resembling the mineral part of the bone such as nanostructure, composition, high specific surface area and porosity. Altogether the material merits further studies in clinical settings.

Acknowledgements

Authors acknowledge the support from:

Programa Nacional de Cooperación Público-Privada - Subprograma INNPACTO (Orden ECC/1345/2012) del Ministerio de Economía y Competitividad, España (Spain). Grant No IPT-2012-0560-010000 "Sil-Oss: Osteoinductive biomaterial for bone regeneration.

The authors wish to thank also to Alfonso Rodríguez and Juan Luis Baldonedo of the ICTS Centro Nacional de Microscopía Electrónica (Spain) for the assistance in the scanning electron microscopy and transmission electron microscopy studies, respectively.

References

- Klein-Nulend J, Bacabac RG, Mullender MG (2005) Mechanobiology of bone tissue. *Pathol Biol (Paris)* 53: 576-580.
- Dahlin C, Johansson A (2011) Iliac crest autogenous bone graft versus alloplastic graft and guided bone regeneration in the reconstruction of atrophic maxillae: A 5-year retrospective study on cost-effectiveness and clinical outcome. *Clin Implant Dent Relat Res* 13: 305-310.
- Chernousova S, Epple M, (2014) Bioactive bone substitution materials. *Adv Biomater Devices Med* 1: 74-87.
- Bose S, Roy M, Bandyopadhyay A (2012) Recent advances in bone tissue engineering scaffolds. *Trends Biotechnol* 30: 546-554.
- Stevens MM (2008) Biomaterials for bone tissue engineering. *Mater Today* 11: 18-25.
- Turri A, Dahlin C (2015) Comparative maxillary bone-defect healing by calcium-sulphate or deproteinized bovine bone particles and extra cellular matrix membranes in a guided bone regeneration setting: an experimental study in rabbits. *Clin Oral Implants Res* 26: 501-506.
- Dorozhkin SV (2007) Calcium orthophosphates. *J Mater Sci Mater Med* 42: 1061-95.
- Vallet-Regí M, González-Calbet JM (2004) Calcium phosphates as substitution of bone tissues. *Prog Solid State Chem* 32: 1-31.
- Arcos D (2014) Calcium Phosphate Bioceramics. In: Vallet-Regí M, editor. *Bioceramics with Clin Appl* (1stedn), Chichester: JohnWiley & Sons Ltd p. 25-71.
- Webster TJ, Ergun C, Doremus RH, Siegel RW, Bizios R (2000) Enhanced functions of osteoblasts on nanophase ceramics. *Biomaterials* 21: 1803-1810.
- Oh S, Oh N, Appleford M, Ong JL (2006) Bioceramics for Tissue Engineering Applications. *A Review Am J Biochem Biotechnol* 2: 49-56.
- Theiss F, Apelt D, Brand B, Kutter A, Zihszky K, et al. (2005) Biocompatibility and resorption of a brushite calcium phosphate cement. *Biomaterials* 26: 4383-4394.
- Tamimi F, Sheikh Z, Barralet J (2012) Dicalcium phosphate cements: Brushite and monetite. *Acta Biomater* 8: 474-487.
- Tamimi F, Le Nihouannen D, Eimar H, Sheikh Z, Komarova S, et al. (2012) The effect of autoclaving on the physical and biological properties of dicalcium phosphate dihydrate bioceramics: brushite vs. monetite. *Acta Biomater* 8: 3161-3169.
- Tamimi F, Torres J, Bassett D, Barralet J, Cabarcos EL (2010) Resorption of monetite granules in alveolar bone defects in human patients. *Biomaterials* 31: 2762-2769.
- Tamimi F, Torres J, Kathan C, Baca R, Clemente C, et al. (2008) Bone regeneration in rabbit calvaria with novel monetite granules. *J Biomed Mater Res A* 87: 980-985.
- Gbureck U, Hölzel T, Klammert U, Würzler K, Müller FA, et al. (2007) Resorbable dicalcium phosphate bone substitutes prepared by 3D powder printing. *Adv Funct Mater* 17: 3940-3945.
- Dorozhkin S V (2013) Calcium orthophosphate-based bioceramics. *Materials (Basel)* 6: 3840-3942.
- Klammert U, Reuther T, Jahn C, Kraski B, Kübler AC, et al. (2009) Cytocompatibility of brushite and monetite cell culture scaffolds made by three-dimensional powder printing. *Acta Biomater* 5: 727-734.
- Habibovic P, Gbureck U, Doillon CJ, Bassett DC, van Blitterswijk CA, et al. (2008) Osteoconduction and osteoinduction of low-temperature 3D printed bioceramic implants. *Biomaterials* 29: 944-953.
- Bohner M, Theiss F, Apelt D, Hirsiger W, Houriet R, et al. (2003) Compositional changes of a dicalcium phosphate dihydrate cement after implantation in sheep. *Biomaterials* 24: 3463-3474.
- Tamimi F, Torres J, Gbureck U, Lopez-Cabarcos E, Bassett DC, et al. (2009) Craniofacial vertical bone augmentation: A comparison between 3D printed monolithic monetite blocks and autologous onlay grafts in the rabbit. *Biomaterials* 30: 6318-6326.
- LeGeros RZ (2008) Calcium phosphate-based osteoinductive materials. *Chem Rev* 108: 4742-4753.
- Hench LL, Polak JM (2002) Third-generation biomedical materials. *Science* 295: 1014-1017.
- Hoppe A, Güldal NS, Boccaccini AR (2011) A review of the biological response to ionic dissolution products from bioactive glasses and glass-ceramics. *Biomaterials* 32: 2757-2774.
- Yamaguchi M (1998) Role of zinc in bone formation and bone resorption. *J Trace Elem Exp Med* 11:119-35.
- Bose S, Fielding G, Tarafder S, Bandyopadhyay A (2013) Understanding of dopant-induced osteogenesis and angiogenesis in calcium phosphate ceramics. *Trends Biotechnol* 31: 594-605.
- Lakhkar NJ, Lee IH, Kim HW, Salih V, Wall IB, et al. (2013) Bone formation controlled by biologically relevant inorganic ions: role and controlled delivery from phosphate-based glasses. *Adv Drug Deliv Rev* 65: 405-420.
- Seo HJ, Cho YE, Kim T, Shin HI, Kwun IS (2010) Zinc may increase bone formation through stimulating cell proliferation, alkaline phosphatase activity and collagen synthesis in osteoblastic MC3T3-E1 cells. *Nutr Res Pract* 4: 356-361.
- Hadley KB, Newman SM, Hunt JR (2010) Dietary zinc reduces osteoclast resorption activities and increases markers of osteoblast differentiation, matrix maturation, and mineralization in the long bones of growing rats. *J Nutr Biochem* 21: 297-303.
- Moonga BS, Dempster DW (1995) Zinc is a potent inhibitor of osteoclastic bone resorption in vitro. *J Bone Miner Res* 10: 453-457.
- Garcia de Castro A, Carrodeguas GR, Padilla S, Contreras AN (2010) Bone regeneration materials based on combinations of monetite and other bioactive calcium and silicon compounds, WO 2010092001.
- De La Torre AG, Bruque S, Aranda MAG (2001) Rietveld quantitative amorphous content analysis. *J Appl Crystallogr* 34: 196-202.
- Toby BH, Von Dreele RB (2013) GSAS-II: The genesis of a modern open-source all purpose crystallography software package. *J Appl Crystallogr* 46: 544-549.
- Holland TJB, Redfern SAT (1997) Unit cell refinement from powder diffraction data: The use of regression diagnostics. *Mineral Mag* 61: 65-77.
- Mosmann T (1983) Rapid colorimetric assay for cellular growth and survival: application to proliferation and cytotoxicity assays. *J Immunol Methods* 65: 55-63.
- Nuss KM, Auer JA, Boos A, von Rechenberg B (2006) An animal model in sheep for biocompatibility testing of biomaterials in cancellous bones. *BMC Musculoskelet Disord* 7: 67.
- Petrov I, Soptrajanov B, Fuson N, Lawson JR (1967) Infra-red investigation of

- dicalcium phosphates. *Spectrochim Acta Part A Mol Spectrosc* 23: 2637-2646.
39. LeGeros RZ1 (1991) Calcium phosphates in oral biology and medicine. *Monogr Oral Sci* 15: 1-201.
40. Vallet-Regí M, Rámila A, Padilla S, Muñoz B (2003) Bioactive glasses as accelerators of apatite bioactivity. *J Biomed Mater Res A* 66: 580-585.
41. Rothwell WP, Waugh JS, Yesinowski JP (1980) High-resolution variable-temperature phosphorus-31 NMR of solid calcium phosphates. *J Am Chem Soc* 102: 2637-2643.
42. Louati B, Hlél F, Guidara K, Gargouri M (2005) Analysis of the effects of thermal treatments on CaHPO₄ by 31P NMR spectroscopy. *J Alloys Compd* 394: 13-18.
43. Sudarsanan K, Young RA (1969) Significant precision in crystal structural details. Holly Springs hydroxyapatite. *Acta Crystallogr B* 25:1534-1543.
44. Combes C, Rey C (2010) Amorphous calcium phosphates: synthesis, properties and uses in biomaterials. *Acta Biomater* 6: 3362-3378.
45. Engelhardt G (2007) Silicon-29 NMR of Solid Silicates. *eMagRes*.
46. Mosselmans G, Biesemans M, Willem R, Wastiels J, Leermakers M, et al. (2007) Thermal hardening and structure of a phosphorus containing cementitious model material?: Phosphoric acid-wollastonite. *J Therm Anal Calorim* 88: 723-729.
47. Dorozhkin S V (2012) Nanodimensional and nanocrystalline calcium orthophosphates. *Am J Biomed Eng* 2: 48-97.
48. Webster TJ, Ergun C, Doremus RH, Siegel RW, Bizios R (2001) Enhanced osteoclast-like cell functions on nanophase ceramics. *Biomaterials* 22: 1327-1333.
49. Karageorgiou V, Kaplan D (2005) Porosity of 3D biomaterial scaffolds and osteogenesis. *Biomaterials* 26: 5474-5491.
50. Woodard JR, Hilldore AJ, Lan SK, Park CJ, Morgan AW, et al. (2007) The mechanical properties and osteoconductivity of hydroxyapatite bone scaffolds with multi-scale porosity. *Biomaterials* 28: 45-54.
51. Lan LeVengood SK, Polak SJ, Wheeler MB, Maki AJ, Clark SG, et al. (2010) Multiscale osteointegration as a new paradigm for the design of calcium phosphate scaffolds for bone regeneration. *Biomaterials* 31: 3552-3563.
52. Barradas AM, Yuan H, van Blitterswijk CA, Habibovic P (2011) Osteoinductive biomaterials: Current knowledge of properties, experimental models and biological mechanisms. *Eur Cell Mater* 21: 407-429.
53. Yuan H, Kurashina K, de Bruijn JD, Li Y, de Groot K, et al. (1999) A preliminary study on osteoinduction of two kinds of calcium phosphate ceramics. *Biomaterials* 20: 1799-1806.
54. Zhao X, Heng BC, Xiong S, Guo J, Tan TT, et al. (2011) In vitro assessment of cellular responses to rod-shaped hydroxyapatite nanoparticles of varying lengths and surface areas. *Nanotoxicology* 5: 182-194.
55. Jugdaohsingh R1 (2007) Silicon and bone health. *J Nutr Health Aging* 11: 99-110.
56. Carlisle EM (1970) Silicon: a possible factor in bone calcification. *Science* 167: 279-280.
57. Damen JJ, Ten Cate JM (1992) Silica-induced precipitation of calcium phosphate in the presence of inhibitors of hydroxyapatite formation. *J Dent Res* 71: 453-457.
58. Maeno S, Niki Y, Matsumoto H, Morioka H, Yatabe T, et al. (2005) The effect of calcium ion concentration on osteoblast viability, proliferation and differentiation in monolayer and 3D culture. *Biomaterials* 26: 4847-4855.
59. Marie PJ1 (2010) The calcium-sensing receptor in bone cells: a potential therapeutic target in osteoporosis. *Bone* 46: 571-576.
60. Valerio P, Pereira MM, Goes AM, Leite MF (2009) Effects of extracellular calcium concentration on the glutamate release by bioactive glass (BG60S) preincubated osteoblasts. *Biomed Mater* 4: 045011.
61. Xynos ID, Edgar AJ, Buttery LD, Hench LL, Polak JM (2001) Gene-expression profiling of human osteoblasts following treatment with the ionic products of Bioglass 45S5 dissolution. *J Biomed Mater Res* 55: 151-157.
62. Gorostovich AA, Roether JA, Boccaccini AR (2010) Effect of bioactive glasses on angiogenesis: a review of in vitro and in vivo evidences. *Tissue Eng Part B* Rev 16: 199-207.
63. Bellows CG, Heersche JN, Aubin JE (1992) Inorganic phosphate added exogenously or released from βglycerophosphate initiates mineralization of osteoid nodules in vitro. *Bone Miner* 17: 15-29.
64. Penido MG, Alon US (2012) Phosphate homeostasis and its role in bone health. *Pediatr Nephrol* 27: 2039-2048.
65. Beck GR Jr, Moran E, Knecht N (2003) Inorganic phosphate regulates multiple genes during osteoblast differentiation, including Nrf2. *Exp Cell Res* 288: 288-300.
66. Julien M, Khoshniat S, Lacreusette A, Gatius M, Bozec A, et al. (2009) Phosphate-dependent regulation of MGP in osteoblasts: role of ERK1/2 and Fra-1. *J Bone Miner Res* 24: 1856-1868.
67. Padilla S, Román J, Carenas A, Vallet-Regí M (2005) The influence of the phosphorus content on the bioactivity of sol-gel glass ceramics. *Biomaterials* 26: 475-483.
68. Tapiero H, Tew KD (2003) Trace elements in human physiology and pathology: zinc and metallothioneins. *Biomed Pharmacother* 57: 399-411.
69. Prasad AS (1991) Discovery of human zinc deficiency and studies in an experimental human model. *Am J Clin Nutr* 53: 403-412.
70. Pina S, Vieira SI, Rego P, Torres PM, da Cruz e Silva OA, et al. (2010) Biological responses of brushite-forming Zn- and ZnSr- substituted beta-tricalcium phosphate bone cements. *Eur Cell Mater* 20: 162-177.
71. Kawamura H, Ito A, Miyakawa S, Layrolle P, Ojima K, et al. (2000) Stimulatory effect of zinc-releasing calcium phosphate implant on bone formation in rabbit femora. *J Biomed Mater Res* 50: 184-190.
72. Li X, Sogo Y, Ito A, Mutsuzaki H, Ochiai N, et al. (2009) The optimum zinc content in set calcium phosphate cement for promoting bone formation in vivo. *Mater Sci Eng C Mater Biol Appl* 29: 969-975.
73. EFSA NDA Panel (EFSA Panel on Dietetic Products N and A) (2014) Scientific Opinion on Dietary Reference Values for zinc. *EFSA J* 12: 3844.
74. Ginebra MP, Espanol M, Montufar EB, Perez RA, Mestres G (2010) New processing approaches in calcium phosphate cements and their applications in regenerative medicine. *Acta Biomater* 6: 2863-2873.
75. Galindo-Moreno P, Hernández-Cortés P, Mesa F, Carranza N, Juodzbaly G, et al. (2013) Slow resorption of anorganic bovine bone by osteoclasts in maxillary sinus augmentation. *Clin Implant Dent Relat Res* 15: 858-866.
76. Schlegel KA, Fichtner G, Schultze-Mosgau S, Wiltfang J (2003) Histologic findings in sinus augmentation with autogenous bone chips versus a bovine bone substitute. *Int J Oral Maxillofac Implants* 18: 53-58.
77. Oonishi H, Kushitani S, Yasukawa E, Iwaki H, Hench LL, et al. (1997) Particulate bioglass compared with hydroxyapatite as a bone graft substitute. *Clin Orthop Relat Res*: 316-325.
78. Jones JR1 (2013) Review of bioactive glass: from Hench to hybrids. *Acta Biomater* 9: 4457-4486.
79. Apelt D, Theiss F, El-Warrak AO, Zlinszky K, Bettschart-Wolfisberger R, et al. (2004) In vivo behavior of three different injectable hydraulic calcium phosphate cements. *Biomaterials* 25: 1439-1451.